INTERNATIONAL JOURNAL OF PRECISION ENGINEERING AND MANUFACTURING Vol. 16, No. 4, pp. 619-627 APRIL 2015 / 619
DOI: 10.1007/s12541-015-0083-4 ISSN 2234-7593 (Print) / ISSN 2005-4602 (Online)

Deformation Analysis of Rectangular Channel Structures in Micro Pattern Machining

Thanh-Hung Duong[1] and Hyun-Chul Kim[1,#]

1 High Safety Vehicle Core Technology Research Center, Department of Mechanical and Automotive Engineering, Inje University, 197, Inje-ro, Gimhae-si, Gyeongsangnam-do, 621-749, South Korea
Corresponding Author / E-mail: mechkhc@inje.ac.kr, TEL: +82-55-320-3988, FAX: +82-55-324-1723

KEYWORDS: Ultra-precision machining, Micro channel, Machining process, Deformation, Diamond machining

In micro pattern machining, rectangular channel structures having high aspect ratio can be easily deformed because the cutting force perpendicular to the moving direction of the diamond tool pushes the channel structure. In order to prevent such deformation, conservative cutting conditions that can reduce the cutting force are applied, but make great sacrifices in productivity. Therefore, it is necessary to study the deformation behavior of micro channels to determine optimum cutting conditions. This paper presents a theoretical prediction solution for the deformation of the micro rectangular channels. To obtain maximum principle stress and deflection of micro rectangular pattern, the used model was a cantilever beam with a distributed load. Furthermore, for verifying this solution, FEM analysis and experiments have been carried out to rectangular patterns by diamond machining. The maximum error between the predicted deformation and experimental deformation was approximately 5mm, which means that this prediction solution works well.

Manuscript received: June 12, 2014 / Revised: September 23, 2014 / Accepted: December 10, 2014

1. Introduction

Recently, research which aiming to fabricate plastic optical elements with micro-structures at high efficiency but low cost is grossing and is considered as a current trend.[1] These optical elements are intensively used commonly in optics, displays, communications, electronics, and fuel cell industries. The most popular examples of using these elements include concave and convex plastic lenses, Light Guide Panel.[2] In producing plastic optical elements with micro-structures, one of the most common methods is injection molding technique. A simple summary of injection molding method is shown in Fig. 1. This method consists of mold filling, packing, and cooling stages.[3] Various kind of materials are applied for the optical mold such as electroless nickel-phosphorous (Ni-P) plated mold steels, aluminum alloys and copper alloys.[4] These materials are machined using a single-point diamond tool on ultra-high precision machines. This process enables the shaping of the inserting mold to have complicated forming surfaces in order to give desired optical characteristics. However, diamond ultra-precision machining of brass that carries high aspect ratio micro-patterns involves lots of problem in terms of deformation. These problems ultimately result in badly quality molds. Fig. 2 illustrates the state of molds after deformation occurs. As a result, a large deformation was observed from our experiment in fabricating the rectangular micro pattern with high aspect ratio on the mold surface. To prevent such deformation, conservative cutting conditions that can reduce the cutting force are used. However, these methods require a lot of works and reduce the productivity. Thus, a proper selection of machining process conditions is an important prerequisite for product quality assurance, machining cost reduction, productivity increase, and assistance in computer-aided process planning.[5,6]

Therefore, it is necessary to study the deformation behavior of micro patterns in diamond precision machining to avoid deformation and to determine possible optimum cutting conditions. Researchers had tried to approach this behavior by various methods from theory to simulation and experiment. To analyze three dimensions cutting, the numerical approaches based on the Finite Element Method (FEM) as the closest solutions are considered.[7] Bacaria applied the transient numerical models of metal cutting by using the Johnson-Cook's rupture criterion. Pantale used the ALE 3D model for orthogonal and oblique metal cutting processes. Both of them showed a very good agreement of FEM with experimental results. But for orthogonal cutting, the radial cutting force was assumed to equal zero, hence, the deformation of

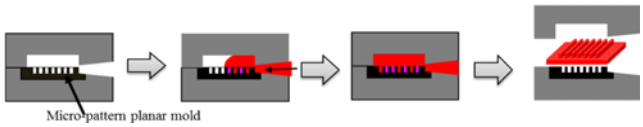

Fig. 1 Micropattern injection molding

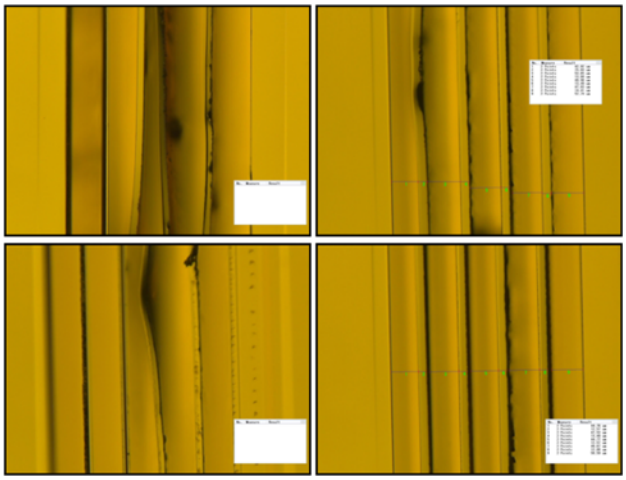

Fig. 2 Deformation phenomenon

pattern was neglected. On the other hand, the micro pattern with high aspect ratio is a typical type of thin walled structures. Ning et al applied the FEM method to quantitative analyze and calculate the deformation in the process of CNC milling. Because of the coincidence between FEM and practical results, it proved that based on the deformation calculation a compensation method can be adopted to produce precise thin-walled components. Rai et al. presented a comprehensive FEM based milling process plan verification model to predict the part thin wall deflections and elastic-plastic deformations during machining. But these FEM were applied for milling machining not diamond machining. To the best of the author's knowledge, there has not yet been a study based on FEM to estimate the deformation of micro pattern in diamond machining process.

In this paper, a FEM analysis of deformation behavior of high aspect ratio micro channels in diamond ultra-precision machining was presented. The shape of cutting tool is rectangle. Due to the easy to use and quick set up feature, a standard package of ANSYS Workbench v12 was chosen as the FEM software medium. Furthermore, to verify FEM analysis method, several experiments in diamond ultra-precision cutting were carried out and are compared.

2. Analytical Method

2.1 Deformation sources

In micro channel fabrication, favorite cutting mode for rectangular pattern is plunge cutting, as shown in Fig. 3. Grooves are machined completely and sequentially. This mode guarantees the accuracy of pattern by reducing positioning errors.

In our previous study, the source of lateral deformation was verified

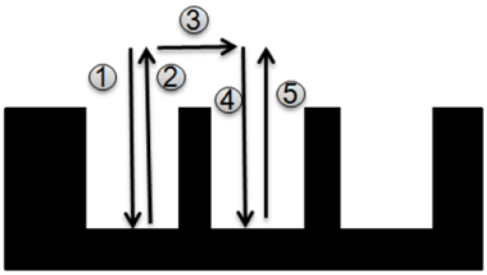

Fig. 3 Plunge cutting mede

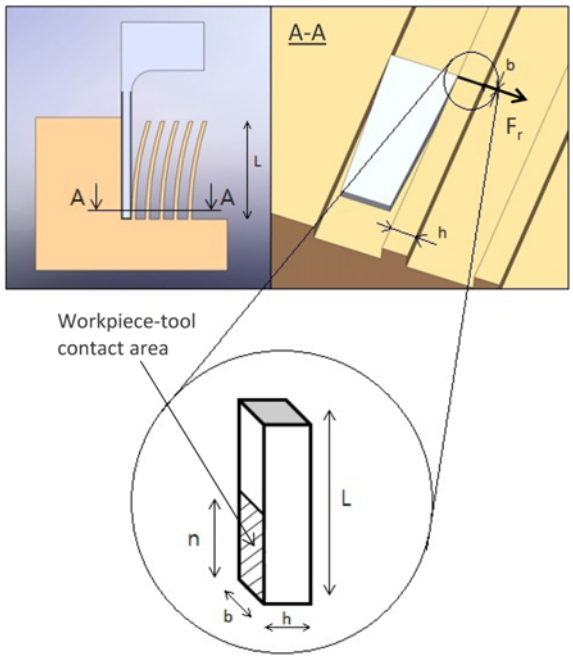

Fig. 4 Radial force acts on the side face of micro channel

as cutting force.[8] During cutting process, radial cutting force F_r, of three cutting force components causes a normal stress on side face of micro pattern, as shown in Fig. 4, we call this stress as side stress. Depending on the large of this stress, micro pattern can be deformed. If the side stress excesses the yield strength of workpiece's material, the plastic deformation will occurs. Otherwise, the micro pattern can only be deformed elasticity, this means that the deflection of pattern returns to zero when tool passes over the pattern or there is no contact between tool and micro pattern.

2.2 Proposal theoretical deformation modelling

A micro channel was considered as consisting of many rectangular thin plates, as shown in Fig. 5. All these plates have the same dimensions: height L, width h and thickness b. During machining process of cutting step i, the cutting tool moves along the X-axis, from 0 to L_w. In case where the lateral deformation occurs, it grows along the micro channel. For the sake of simplicity, we assumed that there is no interaction between these plates, they are deformed separately. Because all thin plates have the same dimension and the cutting force is kept constant value in one cutting step, the maximum deflection of them

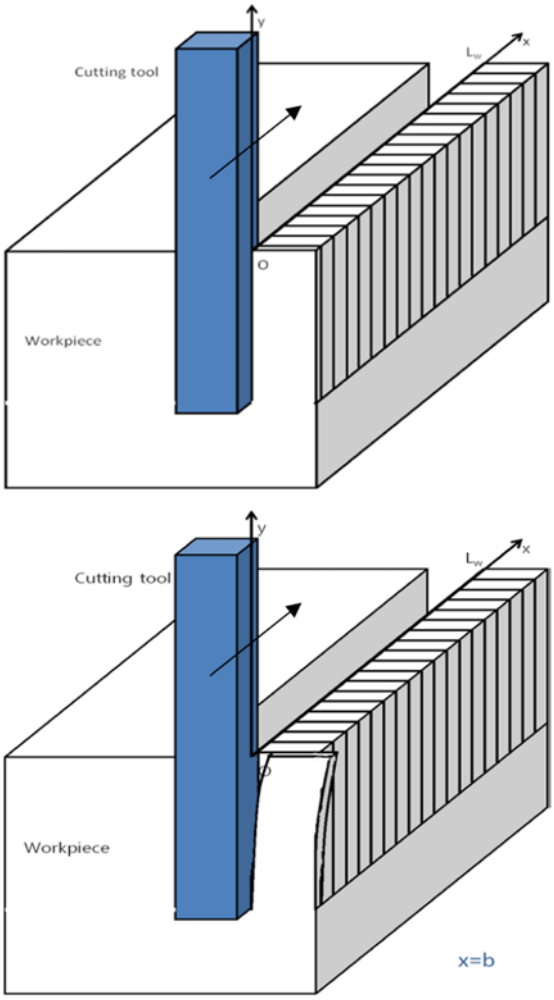

Fig. 5 The modeling of the deformation of a micro pattern

will be the same value d_i. Hence, the maximum deflection of a thin plate equals the maximum deflection of the micro pattern.

On the other hand, the thin plate have many similar features with cantilever beam. The width/height h/L ratio and the thickness/height b/L of a thin plate are significantly small number. Plus, the radial force is perpendicular to the thin plate. In case where deformation occurs, the bottom of a thin plate is laterally and rotationally fixed, and the top of a thin plate is free to move along the Z-axis. Therefore, we decided to use cantilever beam to calculate deformation of thin plate. In addition, the radial forces F_r was converted to the distributed load ω. Besides, after the tool passes, the beam is unloaded; it still has the trend of recover to its original position but it was plastically deformed, hence, the beam move recover but not fully.[11] This phenomenon is called springback, as illustrated in Fig. 7. Springback behavior depends on material properties, geometry and tooling dimensions. Kalpakjian and Schimid have estimated the initial radius/final radius ratio by the following equation:[12]

$$\frac{R_i}{R_f} = 4\left(\frac{R_i Y}{Et}\right)^3 - 3\left(\frac{R_i Y}{Et}\right) + 1 \quad (1)$$

For simplification, in order to predict deformation of the rectangular pattern, the following assumptions are applied:

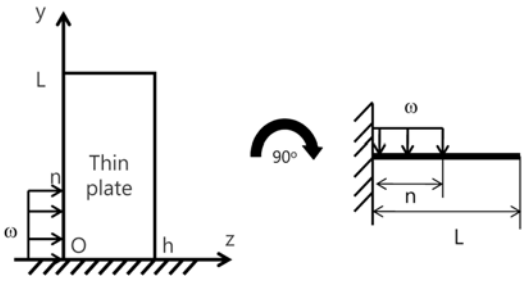

Fig. 6 The uniform distributed load on the cantilever beam

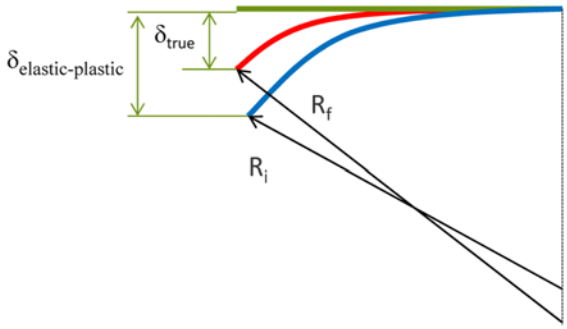

Fig. 7 Springback phenomenon

(1) The distributed load on the contact area is uniform linear.
(2) The displacement of every point on the beam does not change along the thickness.
(3) There is no interaction between the chip flow and the rectangular pattern.
(4) The cutting type is orthogonal cutting.

Based on the proposal deformation modeling, Fig. 8 is a flow chart of deformation calculation of rectangular patterns. The input data consists of machining conditions, material's properties and cutting tool conditions. To machine a micro pattern with the height L, we will need k cutting steps and k =L/d, where d is depth of cut. At the cutting step i, the cutting force is calculated by applying a modified Merchant's method, then it is converted to distributed load and estimate side stress. Comparing the side stress and yield strength of a workpiece material determines the type of deformation: elastic or plastic. If only elastic deformation occurs, when the tool passes over, patterns return to its original position and deflection of this step equal zero. Otherwise, in cases where the side stress surpasses workpiece's yield strength, the pattern is deformed plastically and its deflection will be used for calculating the deflection of the next step, i+1 and be accumulated in total maximum deflection. These steps are repeated until the tool reaches the required depth of pattern.

2.3 Mathematics

2.3.1 Cutting force and distributed load

With a high tech measurement instrument, the cutting force and thrust force of a cutting tool can be measured accurately without any difficulty. But in the case of the radial force, it's hard to get the exact value because it's relatively small. In theory, the Merchant's model is considered the most famous approach for cutting force estimation and

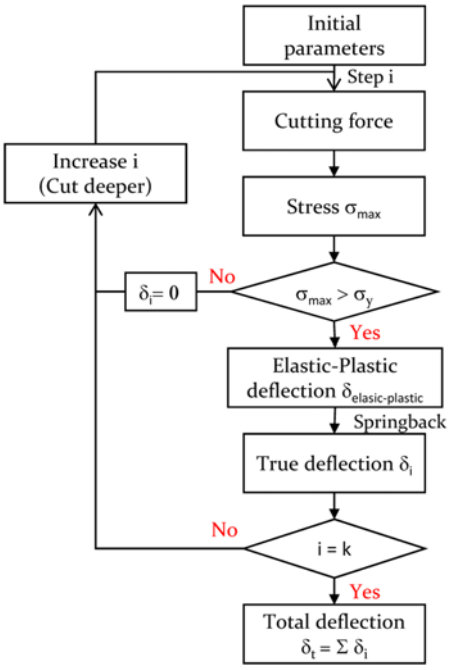

Fig. 8 Flow chart to calculate deformation

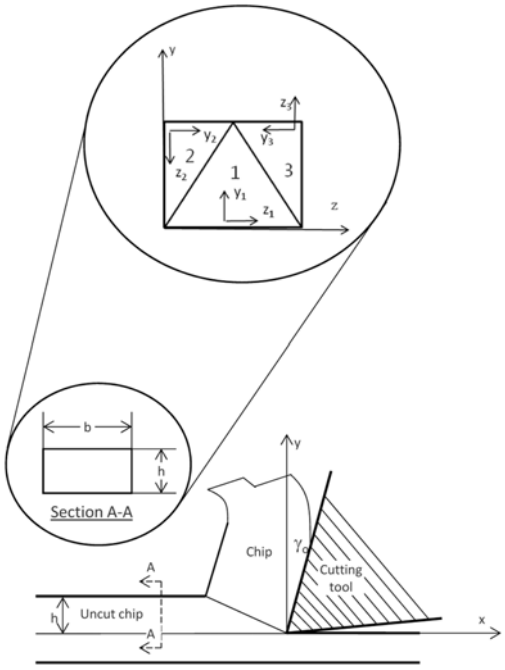

Fig. 9 Cross section of a divided, uncut chip

it is widely used in introductive courses on machining.[7] But in orthogonal cutting, this model assumed that the radial force equals zero. Therefore, a modified method has been proposed: the dividing solution. The cross-section of an uncut chip will be divided into several parts. Each part will be applied to the Merchant's theory to determine the local cutting force and local thrust force. The total cutting force will be determined by combining these local forces.

There are many ways to divide the rectangular uncut chip. Because the cutting is done by 3 tool edges, the dividing method, as shown in Fig. 9 - three pieces linearly divided - was chosen for calculation in this paper. The study on the effectiveness and differences of the dividing method will be discussed in future. By using Merchant's equation, the local cutting force of 3 pieces can be expressed as

$$\vec{F}_{local1} = \begin{bmatrix} F_{1c} \\ F_{1t} \end{bmatrix} = \begin{bmatrix} \dfrac{\cos(\beta-\gamma_o)}{\cos(\phi_o+\beta-\gamma_o)} \\ \dfrac{\sin(\beta-\gamma_o)}{\cos(\phi_o+\beta-\gamma_o)} \end{bmatrix} \frac{\tau_s bh}{2\sin(\phi_o)} \tag{2}$$

$$\vec{F}_{local2} = \vec{F}_{local3} = \begin{bmatrix} F_{2c} \\ F_{2t} \end{bmatrix} = \begin{bmatrix} \dfrac{\cos(\beta-\gamma_o)}{\cos(\phi_o+\beta-\gamma_o)} \\ \dfrac{\sin(\beta-\gamma_o)}{\cos(\phi_o+\beta-\gamma_o)} \end{bmatrix} \frac{\tau_s bh}{4\sin(\phi_o)} \tag{3}$$

Among 3 cutting force components there is a local thrust force to piece number 3, which acts on the side wall, thus, to calculate the stress that acts on the micro pattern, the thrust force (F_{3t}), a component of piece number 3, is used. This force is converted to a uniform distributed load w, by the following expression:

$$\omega = \frac{F_{3t}}{n} = \frac{1}{n} \times \frac{\sin(\beta-\gamma_o)}{\cos(\phi_o+\beta-\gamma_o)} \times \frac{\tau_s bh}{4\sin(\phi_o)} \tag{4}$$

With distributed load ω, the maximum stress σ_{max} on the cantilever beam, shown in Fig. 4, can be calculated as the following equation:

$$\sigma_{max} = \frac{3\omega\left(\dfrac{n}{h}\right)^2}{b} \tag{5}$$

2.3.2 Maximum deflection

After comparing the maximum side stress with the yield strength, the type of deformation of the workpiece (elastic or plastic deformation) can be determined.

After analyzing the common and different features between elastic mode and plastic mode, in order to calculate easier, the cantilever was divided into two parts based on the position of distributed load, as shown in Fig. 10. The part with distributed load, which is always a straight beam in the beginning of every step, will be bent. The length of this part equals the height of contact area n, and its deflection at the tip is d_{i1}. The other part, which has been bended (or not) in the previous steps, will not be deflected anymore, but it will be rotated at an angle α_i due to the deformation of the part with distributed load. This rotation will create a deflection δ_{i2}. Naturally, the deflection of step i will be the sum of those two deflections δ_{i1} and δ_{i2}

$$\delta_i = \delta_{i1} + \delta_{i2} \tag{6}$$

2.3.2.1 Part I with distributed load

The part with distributed load always straight at the beginning of every cutting step and is bent at the ending. The angle of rotation at tip θ and the maximum deflection δ at the free end of cantilever are two factor which will be determined.[10]

When the maximum moment in the beam exceeds the yield moment M_y, the beam will have two regions: (1) a region of fully elastic behavior, and (2) a region of elastic-plastic behavior, as shown in the

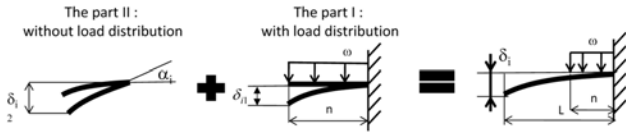

Fig. 10 Two parts of a cantilever: with distributed load and without distributed load

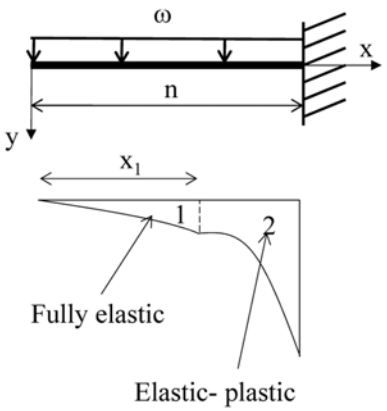

Fig. 11 Two regions of a cantilever beam: full elastic and elastic-plastic

Fig. 11.

The angle at the end of the beam θ is equal to the area of the curvature diagram:

$$\theta = \int_0^{x_1} \frac{\omega x^2 dx}{2EI} + \int_{x_1}^{n} \frac{\kappa_y dx}{\sqrt{3-2\frac{M}{M_y}}} = \frac{\omega x_1^3}{6EI} + \kappa_y \sqrt{\frac{M_y}{\omega}} \left(\sin^{-1}\left(n\sqrt{\frac{\omega}{3M_y}} \right) - \sin^{-1}\left(x_1 \sqrt{\frac{\omega}{3M_y}} \right) \right) \tag{7}$$

And we also have the deflection at the end of the beam calculated δ from the second curvature-area theorem as follows:

$$\delta = \int_0^{x_1} \frac{\omega x^3 dx}{2EI} + \int_{x_1}^{n} \frac{\kappa_y x dx}{\sqrt{3-2\frac{M}{M_y}}} = \delta_y \frac{\omega_y}{\omega} \left(2 - \sqrt{3-2\frac{\omega}{\omega_y}} \right) \tag{8}$$

Next step is springback calculation. Compared to the length of beam L, the deflection at the tip is relatively small. So the cantilever beam is considered as an arc of a circle, as shown in Fig. 12. Hence, the initial radius R_i can be calculated as:

$$R_i = \frac{n}{\sin\theta} \tag{9}$$

After determining the final radius R_f by using Eq. (1), we can calculate the true maximum deflection of the part under the distributed load without difficulty, as Eq. (10)

$$\alpha_i = \tan^{-1}\left(\frac{\delta_{i1}}{n} \right) \tag{10}$$

And we can also obtain the rotation angle at the tip of part I (with distributed load) α_i is

$$\delta_{i1} = n\tan\left(\frac{1}{2}\sin^{-1}\left(\frac{n}{R_f} \right) \right) \tag{10}$$

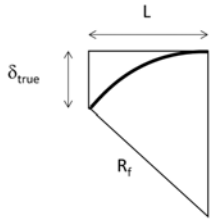

Fig. 12 Arc of a circle

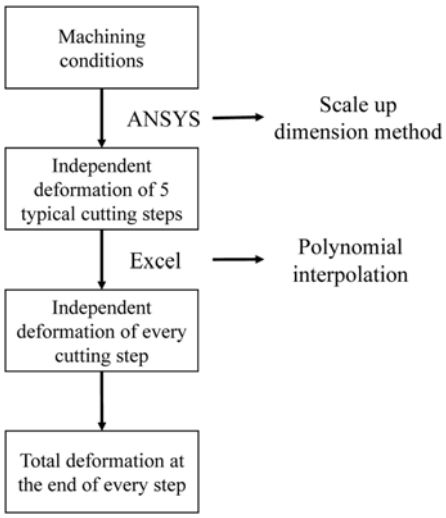

Fig. 13 The flow chart to determine total deformation

2.3.2.2 Part II without distributed load

Unlike the part with load, the part without load could not keep the same form during the machining process. It only rotated angle a_i due to the deformation of the part with load, and this angle is calculated as Eq. (24). Thus, its deflection depends on the deformation of this step and previous steps. It can be expressed by the equation:

$$\delta_{i2} = m\tan\left(\alpha_i + \tan^{-1}\left(\frac{\delta_{i-1}}{m} \right) \right) \tag{11}$$

where m is length of the part without distributed load, δ_{i-1} is deflection of previous steps

In the end, the maximum deflection of the step *i* will be obtained by the sum of the maximum deformation of two parts, as Eq. (6). This calculation procedure has been repeated until the desired height of pattern was achieved.

2.4 The FEM analysis of deformation behavior

Finite element method (FEM) has a great use in modelling orthogonal (2D) and oblique (3D) metal cutting. One of the first FEM models for metal cutting processes is developed by Klamecki.[11] He used an updated Lagrangian elasto-plastic 3D model, but it was limited

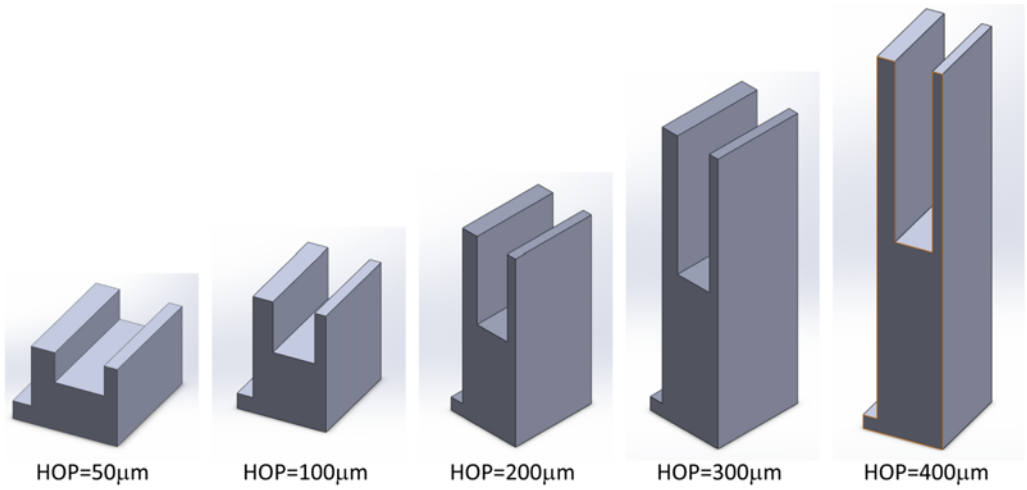

Fig. 14 Five geometrical workpiece models

to the initial stages of chip formation.

With the developments of hardware and commercial FE codes, limitations in modelling and computational problems have been overcome to some extent. Thus, many researchers has focused on special topics of metal cutting. In recent researches, almost all of the metal cutting simulation are made by these softwares: DEFORM 3D, AdvantEdge, ABAQUS, LS-DYNA. But they are expensive and require high skill users. On the other hand, ANSYS is a general-purpose software package designed for analysis using finite elements. Compare to other software, it's more popular, cheaper, especially, the Workbench module is easy to use for everyone. But the main disadvantage is that ANSYS used generally for large scale simulation. In this paper, a strange approach of ANSYS was used in simulating the deformation of the micro patterns in micro grooving process. Computer analysis of the deformation in micro grooving was realized using the ANSYS Workbench v12 software system and its module for structural analysis - Explicit Dynamic.

Base on the proposal theoretical modelling, an analysis procedure was proposed as shown in Fig. 13. We assumed that every cutting step has independent deformation $ä_{inde\ i}$ which can be estimated by using ANSYS. The total deformation at the end of step i+1 equal sum of all previous independent deformation from 1 to i. Firstly, a certain number of typical cutting steps was chosen to analyze in ANSYS. From different cutting steps, workpiece models with different height of pattern were built. In order to be solvable, the original model, which is in micro scale, were be scaled up to millimeter scale models. After obtaining the discrete set of independent deformation by ANSYS simulation, we used polynomial interpolation function in Excel to establish quickly a relationship between height of pattern and independent deformation. Based on this connection, total deformation at the end of every step can be calculated as Eq. (2).

Height of pattern = cutting step i x depth of cut

$$\delta_{inde} = f(hop) \tag{12}$$

$$\delta_{total\ i} = \sum_{j=1}^{i-1} \delta_{inde\ j} = \int_0^i f(hop) \tag{13}$$

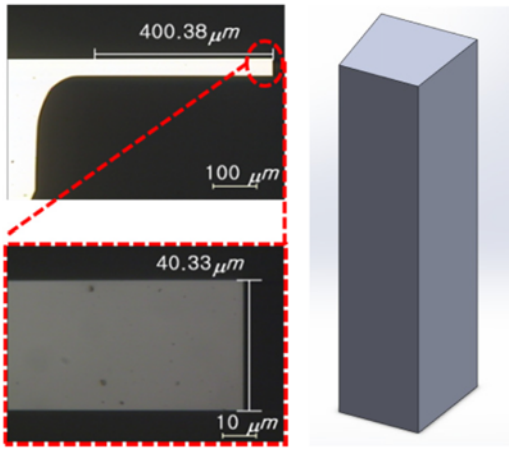

Fig. 15 Real cutting tool and modelling cutting tool

Table 1 Geometrical models

Pattern width	15	μm
Pattern height	50,100,200,300,400	μm
Pattern thickness	100	μm
Cutting tool	400 x 40 x 40 (clearance angle 5°)	μm

2.4.1 FEM geometrical modelling

Based on the above hypothesis, five geometrical workpiece models with different height of patterns have been built, as shown in Fig. 14. The depth of cut was kept constant at 5 mm at grooving process. The middle of the machining step is chosen to simulate. Thus, a groove, which has a height equals to half of the pattern height, is created. This groove's width has the same width of cutting tool. In the other hand, based on the diamond tool, geometrical tool model was also built as shown in Fig. 15. Table 1 shows a dimension of all five geometrical models.

2.4.2 Meshing and boundary conditions

To reduce the simulation calculation time, we concentrated on meshing the area around the contact between tool and workpiece as

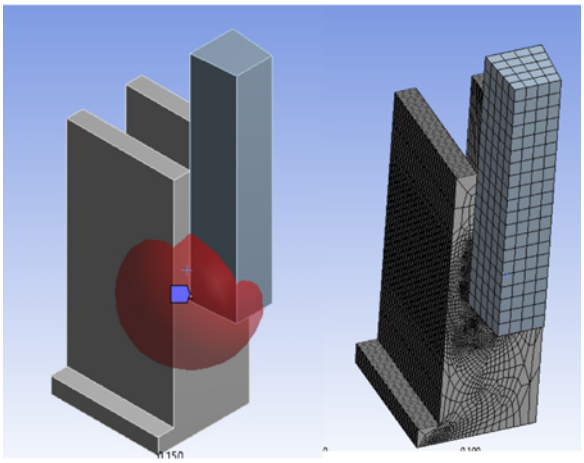

Fig. 16 Meshing for 200mm pattern height case

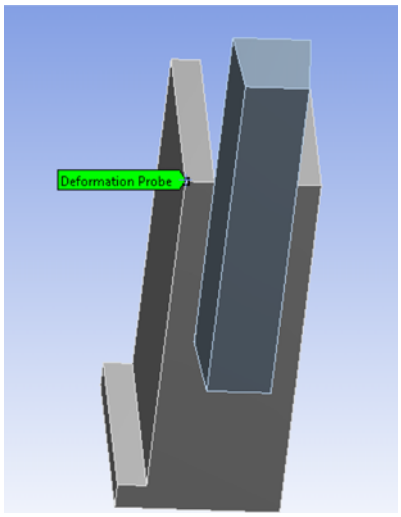

Fig 17 Deformation probe on the workpiece

detailed as possible, as shown in Fig. 16. For example, total number of elements is 147950 for the 200mm of pattern height case.

The next step is choosing the materials for cutting tool part and workpiece part. As mimic the experiment conditions, workpiece and cutting tool's material are brass and diamond. The mechanical properties of parts are applied by using the properties of material used in experiment, which will be presented in "Experiment setup" chapter. After that, for the boundary condition, three bottom faces of workpiece will be considered as fixed support. And the velocity of cutting tool is assigned 100 mm/s, the same value as real machining conditions.

The output of simulation, obviously, is pattern deformation, especially the deformation at the top of pattern. A probe was attached to the vertex of pattern top, to obtain the maximum deflection of pattern, as shown in Fig. 17. The end time of analysis was set as 0.1 second. The Fig. 18 shows a directional deformation of 200 mm height of pattern case. And Table 2 shows the simulation results of five models. By using Excel, a relation between independent deformation and height of pattern was established in form of a polynomial formula, as shown in Fig. 19.

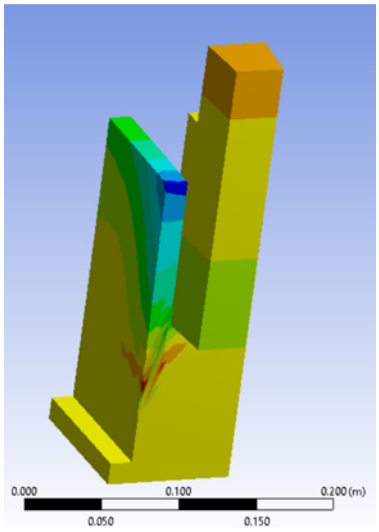

Fig. 18 Directional deformation of 200 mm height of pattern case

Table 2 Simulation results and total deformation estimation

Height of pattern (μm)	Independent deformation (μm)	Total deflection (μm)
50 μm	0.0127	0.6025
100 μm	0.0248	2.98
200 μm	0.0513	12.16
300 μm	0.0836	25.74
400 μm	0.0927	41.92

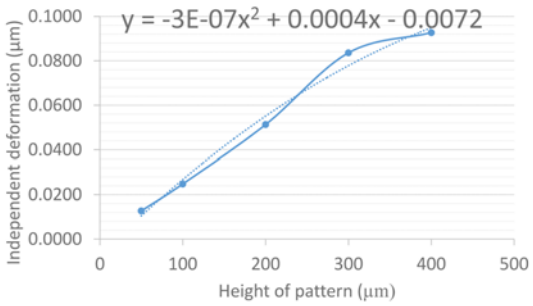

Fig. 19 Relationship between independent deformation and height of pattern

$$\delta_{inde} = -3\times10^{-7}\times hop^2 + 0.0004\times hop - 0.0072 \quad (14)$$

$$\delta_{total} = \int_0^{hop} \delta_{inde} = -1\times10^{-7}\times hop^3 + 0.0002\times hop^2 - 0.0072\times hop \quad (15)$$

3. Experience and Discussion

To validate the simulation solution in this paper, the deflection of micro rectangular patterns and the cutting force were measured by tool dynamometer. This experiment was carried out by grooving machine with diamond cutting tool. In order to avoid flank wear, rake angle is zero and diamond is chosen as cutting tool materials.[12] The grooving

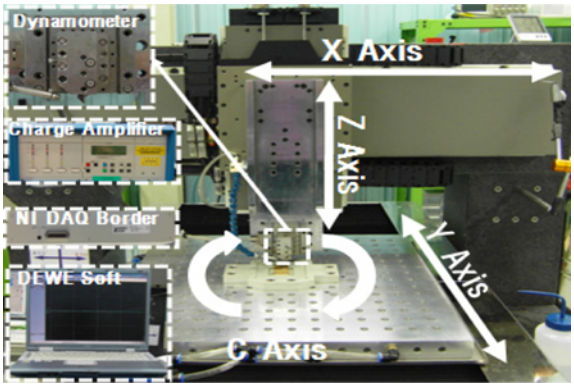

Fig. 20 Grooving machine, measurement tools

machine and the measurement tools are shown in the Fig. 20. The machining system has four axes of driving system: X-, Y-, Z- axis and C- axis. Fundamental machining experiments were carried out by shaping process with single point diamond tool, continuously increasing the cutting depth by 5 mm. During the machining processes, the dynamometer measured three components of cutting force. The output signal was amplified by a charge amplifier and was transmitted to a computer through a NI-DAQ border. Software DEWE was used to analyze the measured data.

Table 3 lists the machining conditions for the experiment. The workpiece is 6:4 Brass, which is used for micro pattern plate mold in industry, its characteristics are shown in Table 3. The workpiece's material is also called Muntz metal - C2800. The true yield strength was obtained by the micro indentation machine MICRO-AIS of Frontics. The height of pattern was different for each experiment, from 50 mm to 400 mm.

After machining, the maximum deflections of 5 different molds were measured from the front view and top view by using SEM, as shown in Fig. 21. There was no deformation occurred in the case of 50 and 100 mm heights of pattern, all patterns kept their original shape. In the contrary, the other cases had uniform deformations, plus when the height of pattern increased, the deflection increased. Hence, the maximum deflection measurement 55.65 mm was obtained from the mold that had the highest pattern.

The comparison of FEM simulation, theory and experiment is

Table 3 Machining condition

Parameter	Description
Machine tool	Planer (900×900×100 stroke)
Cutting tool	W40μm, L400μm, A0 Diamond cutting tool
Workpiece	6:4 Brass 30×30 μm
Cutting speed	100 μm/s
Pattern pitch	15 μm
Cutting depth	(2 μm×1)+(5 μm×79)+(3 μm×1)=400 μm
Cutting oil	Mist oil No. 9

Table 4 The mechanical and chemical characteristics of 6:4 Brass

Mechanical properties			
Nominal Yield Strength (MPa)	True Yield Strength (MPa)	Elongation (%)	Hardness (HV)
250	350	55	135
Chemical components (%)			
Cu	Zn	Pb	Fe
60	39	0.3	0.07

shown in the Fig. 22. In term of trend, the simulation and theoretical calculation results are in agreement with the experimental results. When the height of pattern increases, the maximum deformation also increases. But, unlike experiment, both ANSYS simulation and theoretical prediction had deformation in the cases which patterns have 50 and 100 mm height. When compared to the experiment, the maximum error of simulation is 13.74 mm, while theory's is only 5.27 mm, as illustrated in Table 5. They both shows that when the height of pattern increases, the error between experiment and FEM simulation will increase. The biggest error of theory is only 9.4% which is acceptable, but the FEM simulation is larger - 24%. That means the theory part worked well while the FEM simulation method need to be improved.

4. Conclusions

In this paper, a method for quick simulating the deformation of micro patterns in ultra-precision machining was proposed. The deformation analysis by using our method is quick, easy to follow and can be done by an average skilled operator. Together with FEM simulation, theoretical prediction and experimental results showed that the deformation of micro pattern will change with different height of

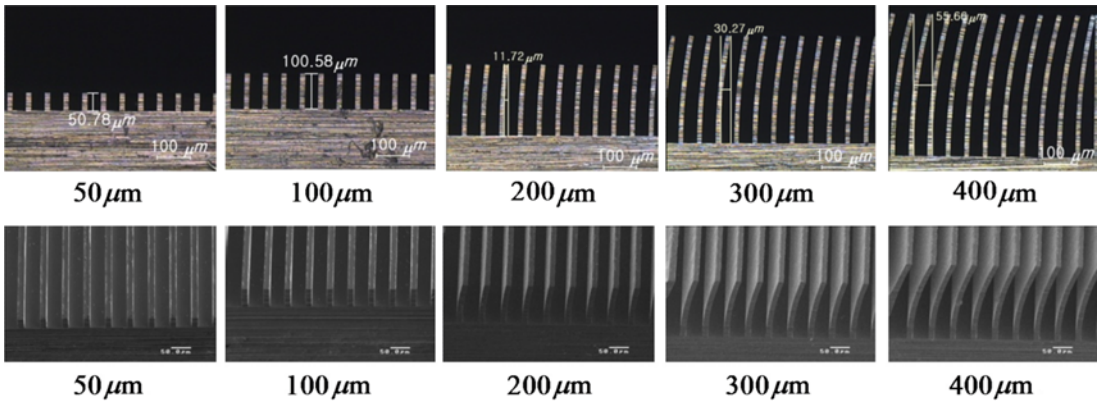

Fig. 21 The front view and top view of five experimental cases

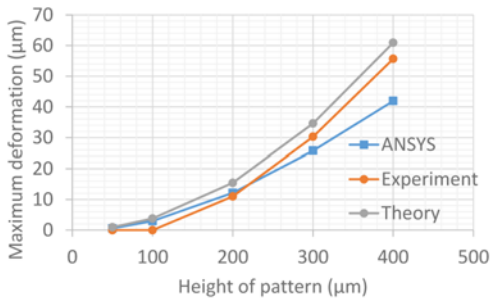

Fig. 22 ANSYS vs Experiment vs Theory in term of maximum deformation

Table 5 The errors of the Theoretical prediction and ANSYS simulation

HOP (μm)	Theory (μm)	FEM simulation (μm)	Experiment (μm)	Theory's error	Simulation's error
50 μm	0.95	0.60	0.00	0.95	0.60
100 μm	3.8	2.98	0.00	3.80	2.98
200 μm	15.43	12.16	11.00	4.43	1.16
300 μm	34.62	25.74	30.27	4.35	-4.53
400 μm	60.93	41.92	55.66	5.27	-13.74

pattern. It suits to what we observed when we tried to produce a higher aspect ratio pattern. When compared to the experiment results, it was shown that the prediction solutions work well. This method can be applied for predicting the maximum deformation of other cutting tool shape, such as triangle, trapezoid.

ACKNOWLEDGEMENT

This research was supported by Basic Science Research Program through the National Research Foundation of Korea (NRF) funded by the Ministry of Education, Science and Technology (2012R1A1B400 1609, 2014R1A1A2053778).

REFERENCES

1. Wang, Y., Zhao, Q., Shang, Y., Lv, P., Guo, B., and Zhao, L., "Ultra-Precision Machining of Fresnel Microstructure on Die Steel Using Single Crystal Diamond Tool," Journal of Materials Processing Technology, Vol. 211, No. 12, pp. 2152-2159, 2011.
2. Abou-El-Hossein, K., Olufayo, O., and Mkoko, Z., "Diamond Tool Wear during Ultra-High Precision Machining of Rapidly Solidified Aluminium RSA 905," Wear, Vol. 302, No. 1, pp. 1105-1112, 2013.
3. Jiang, S., Wang, Z., Zhou, G., and Yang, W., "An Implicit Control-Volume Finite Element Method and Its Time Step Strategies for Injection Molding Simulation," Computers & Chemical Engineering, Vol. 31, No. 11, pp. 1407-1418, 2007.
4. Vancoliie, E., Xiangdong, L., Ling, Y., and Annergren, I., "Materials Selection for Durable Optical Inserts Used in Plastic Lens Moulding," Technical Report (DD/00/009/OTC), SIMTech, Singapore, 2000.
5. Venkata Rao, R. and Kalyankar, V., "Parameter Optimization of Machining Processes using a New Optimization Algorithm," Materials and Manufacturing Processes, Vol. 27, No. 9, pp. 978-985, 2012.
6. Dhananchezian, M., Kumar, M. P., and Sornakumar, T., "Cryogenic Turning of AISI 304 Stainless Steel with Modified Tungsten Carbide Tool Inserts," Materials and Manufacturing Processes, Vol. 26, No. 5, pp. 781-785, 2011.
7. DeVries, W. R., "Analysis of Material Removal Processes," Springer, 1st Ed., pp. 43-54, 1991.
8. Duong, T. H., Kim, H. C., Lee, D. Y., Lee, S. W., Park, E. S., and Je, T. J., "A Theoretical Deformation Prediction of Micro Channels in Ultra-Precision Machining," Int. J. Precis. Eng. Manuf., Vol. 14, No. 2, pp. 173-181, 2013.
9. Lubliner, J., "Plasticity Theory," Courier Dover Publications, pp. 239-245, 2008.
10. Gere, J. M. and Timoshenko, S. P., "Mechanics of Materials," PWS, pp. 306-315, 1997.
11. Klamecki, B. E., "Incipient Chip Formation in Metal Cutting-a Three-Dimension Finite Element Analysis," Ph.D. Thesis, Deparment of Mechanical Engineering, University of Illinois, 1973.
12. El-Hossainy, T., El-Zoghby, A., Badr, M., Maalawi, K., and Nasr, M., "Cutting Parameter Optimization when Machining Different Materials," Materials and Manufacturing Processes, Vol. 25, No. 10, pp. 1101-1114, 2010.